Atmósfera (1992), **5**, *pp. 3-19*

Numerical simulation of dust occurrence in the atmosphere over homogeneous terrain

MOHAMED SAID SALEH EL-MASHJARY

P.O. Box 6002, Khormaksar, ADEN, Democratic Yemen

MARIANO A. ESTOQUE

Department of Meteorology and Oceanography, University of the Philippines, Diliman, Quezon City, Philippines

(Manuscript received June 6, 1990; accepted in final form May 7, 1991)

RESUMEN

Se presenta un modelo numérico de ocurrencia de tormentas de polvo, durante periodos de un flujo dominante fuerte sobre terreno homogeneo. El modelo, que depende del tiempo, incluye una predicción de la temperatura de la superficie de la Tierra con el método de restauración de fuerza. Se incopora la mezcla turbulenta a lo largo de la vertical, a través de una formulación de segundo orden de flujos turbulentos. El modelo se usa para simular la ocurrencia de tormentas de polvo sobre Kuwait, en junio de 1973. La simulación reproduce la variación diurna, observada de las tormentas de polvo. El modelo es también usado para analizar la dependencia de las tormentas de polvo, de la velocidad del viento dominante así como del tamaño de las partículas de polvo. Se describen los resultados del análisis.

ABSTRACT

A numerical model of dust storm occurrence during periods of strong prevailing flow over homogeneous terrain is presented. The model, which is time-dependent, includes a prediction of the Earth's surface temperature with the force-restore method. Turbulent mixing along the vertical is incorporated through a second order formulation of turbulent fluxes. The model is used to simulate the occurrence of dust storms over Kuwait in June 1973. The simulation is able to reproduce the observed diurnal variation of dust storms. The model is also used to analyze the dependence of dust storms on the prevailing wind speed as well as on dust particle size. The results of the analysis are described.

1. Introduction

Dust storms are common in the arid and semi arid lands of the world. These occur under the following conditions:

a. The land surface must be dry and dusty.

b. The wind should reach al least moderate speeds in order to disturb the dust.

c. The air must be unstable, if extensive vertical motion is to occur.

In general there are two types of dust storms. One type (thunderstorm type) is generated by thunderstorms, local or frontal. The local thunderstorms generate dust storms generally in the afternoon, while dust storms which are generated by frontal thunderstorms may occur at any

time of the day. The non-thunderstorm type of dust storm occurs when the large scale synoptic condition is characterized by strong pressure gradients. Under these conditions strong diurnal wind (maximum winds during the day time) variations occur which generate corresponding diurnal occurrences of dust storms. The objective of this study is to develop a numerical model of this non-thunderstorm type of dust storm. This model is used to study the effects of different factors on the characteristics of the dust storms which are generated. The factors are:

a. Wind speed

b. Dust particle size

2. Observational aspects

In this section we will describe, in some detail, the observed characteristics of dust storms of the non thunderstorm type. These dust storms occurred in Kuwait during the period June 17 to 22 1973. This observational study was made by Al-Kulaib (1984). During this period a strong synoptic pressure gradient persisted for several successive days. This was associated with a strong pressure ridge to the west in the Mediterranean region and the usual summer monsoon low over the Arabian Gulf region. This pressure pattern is similar to that in Figure 1, Figs. 2 and 3 show the characteristics of the dust storms based on the autographic records. Figure 2 shows the hourly occurrence of dust storms in Kuwait during the period. Note that dust storms occurred everyday from June 17 to June 21 during the daytime up to the late evening hours.

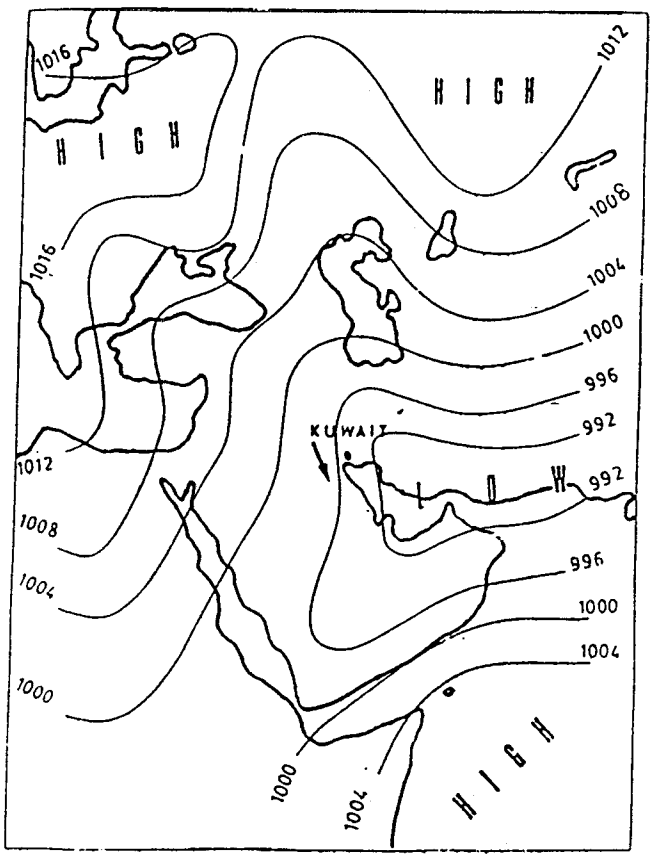

Fig. 1. Surface pressure map showing the typical monsoon low during June and July (after Al-Kulaib, 1984).

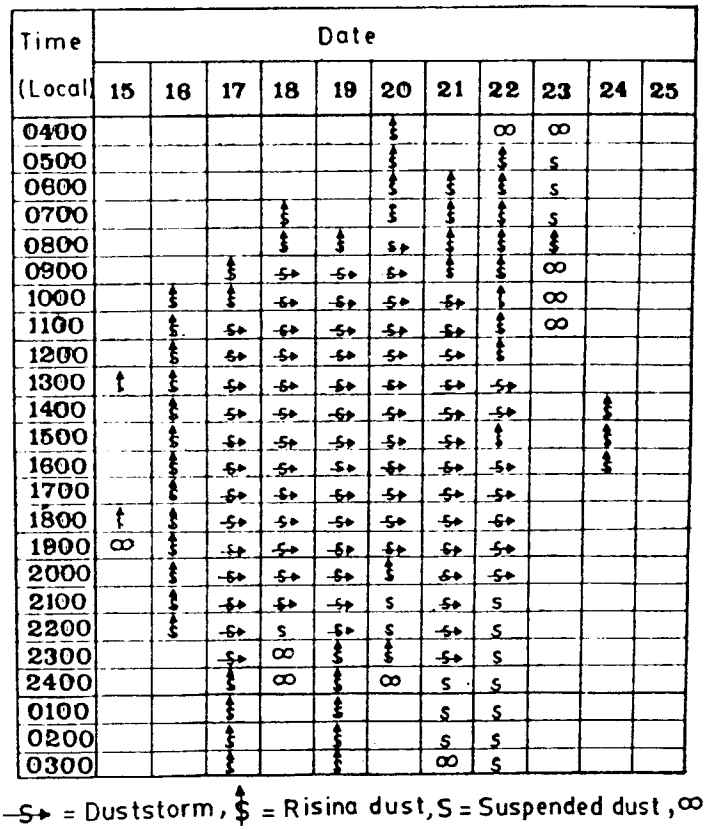

Fig. 2. Dust storm observations at Kuwait International Airport during the period, June 16-22, 1973 (after Al-Kulaib, 1984).

Figure 3 shows the autographic record of the air temperature, surface visibility, wind speed and wind direction. It may be seen from Figure 3, that on June 18, the *shammal* or the northwesterly wind was strong and the visibility dropped to 50 meters, during midday. Wind speed was above 30 mph during the period from 0800 to 1900 LT, and reached 45 mph at 1015 LT, gusting 52 mph.

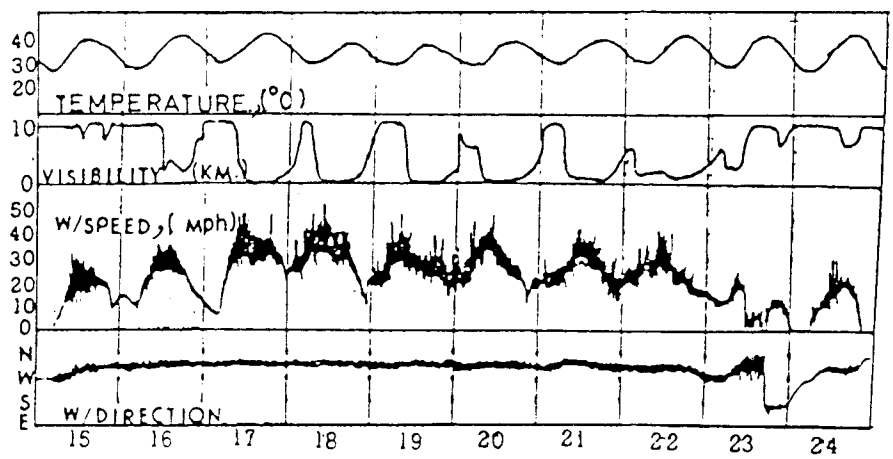

Fig. 3. Surface observations during the occurrence of dust storms for the period, June 15-24, 1973 (after Al-Kulaib, 1984).

On the 19th, the *Shammal* wind decreased slightly as compared to that of the previous days. The wind reached 38 mph at 0830 LT, gusting to 48 mph. Visibility ranged from 100 to 400 meters during the interval, 0900 to 1900 LT, and the sky was obscured during 15 hours.

On the 20th the *Shammal* wind was similar to that which prevailed on the previous day, exceeding 30 mph during a period of 6 hours reaching 36 mph at 1100 LT, gusting to 47 mph. Visibility was below 500 meters during 8 hours.

On the 21st, the *Shammal* markedly by decreased in speed and did not exceed 30 mph for more than two hours. Maximum speed was 34 mph at 1200 LT, gusting to 42 mph. Visibility dropped below 500 meters during 4 hours.

On the 22nd, the *Shammal* wind did not exceed 30 mph for more than one hour. Maximum speed was 34 mph at 1000 LT, gusting to 41 mph. Visibility fell below 500 meters during three hours.

On the 23rd, the *Shammal* wind was light to moderate. Maximum speed was 21 mph at 0800 LT, gusting to 25 mph. Weather improved gradually and visibility improved to 10 km or more by 1200 LT. Wind speed became light and veered to the SE direction at 1700 LT. The sky was not obscured throughout the day while haze particles raised by the previous dust storms remained suspended in the air.

It may be noted that during the six-day period there was a distinct diurnal variation in the wind speed. Maximum wind speeds, dust storms and minimum visibility occurred during the warm periods of the day. On the other hand, light wind speeds occurred together with maximum visibility during the night time. The strong winds during the day time are due to the unstable thermal stratification and the associated intense vertical mixing. The mixing produces downward transport of high momentum to the surface causing the winds to increase. The strong winds generate these diurnal varying dust storms.

3. Numerical model

Very few studies have been made so far on the modelling of dust storms. Among the few models, the one which is most related to our present work is that of Berkofsky (1982). He developed a vertically-integrated model over homogeneous terrain. He used the model to predict the variation of dust concentration with time. Our present model is an attempt to improve Berkofsky's model. We have accomplished this improvement by developing a multi-level model instead of a vertically-integrated model.

The present model consists of two parts. The first part includes equations which simulate the diurnal variation of wind. These equations are based on Estoque's model (1963) of the planetary boundary layer and the model of Estoque and Brumralkar (1969). The second part consists of an equation which predicts the dust concentration. The above models have been extended by introducing the following three modifications:

a. A second order closure scheme in parameterizing the mixing terms due to turbulence.

b. A method for predicting surface temperature, following suggestions by Deardorff (1978).

c. An equation for the rate of change of dust concentration.

The model assumes that the atmosphere consists of two layers. The thin lower layer of 100 meters, which is close to the Earth's surface is considered as the constant flux layer where the fluxes of momentum, heat and dust concentration are assumed to be constant with height. The profiles of temperature, wind and dust concentration in the constant flux layer are calculated by using the profile equations given by Estoque and Brumralkar (1969). The second overlying

layer up to the top of the model is the layer where the prediction equations of the model are integrated.

THE MODEL EQUATIONS

The equations of the present model are as follow:

The momentum equations

$$\frac{\partial U}{\partial t} = f(V - V_g) + \frac{\partial}{\partial Z}(K_z \frac{\partial U}{\partial Z}) \tag{1}$$

$$\frac{\partial V}{\partial t} = F(U_g - U) + \frac{\partial}{\partial Z}(K_z \frac{\partial V}{\partial Z}) \tag{2}$$

The thermodynamic equation

$$\frac{\partial \theta}{\partial t} = \frac{\partial}{\partial Z}(K_z \frac{\partial \theta}{\partial Z}) \tag{3}$$

The conservation for dust concentration

$$\frac{\partial C}{\partial t} = \frac{\partial}{\partial Z}(K_z \frac{\partial C}{\partial Z}) - \Omega \frac{\partial C}{\partial Z} \tag{4}$$

The terms involving k_z represent vertical diffusion. The quantities, U_g and V_g are a measure the pressure gradient force; in the computations they are specified as arbitrary functions of height.

THE DIFFUSION COEFFICIENTS

In the model equations, the turbulent diffusion coefficients are computed, using the second order closure method. The computation is similar to the one described by Gross (1987). The diffusion coefficient is expressed as a function of turbulent kinetic energy (TKE) and computed by the formula:

$$K_z = i\phi^{-1}(a_o E)^{\frac{1}{2}}$$

The stability function Φ is defined by

$\Phi = (1 + \alpha_s \cdot Ri)^{-1}$ for $\frac{\partial \theta}{\partial Z} \geq 0$, stable case

$\Phi = 1 - (\alpha_N \cdot Ri)$ for $\frac{\partial \theta}{\partial Z} < 0$, unstable case

The turbulent length scale is computed by

$$i(Z) = \frac{kZ}{1 + (kZ/i_\infty)}$$

In the computation of K_z in the above paragraph, it is necessary to know the turbulent kinetic energy, E. This quantity is computed using the following equation,

$$\frac{dE}{dt} = K_z\left\{\left[\frac{\partial U}{\partial Z}\right]^2 + \left[\frac{\partial V}{\partial Z}\right]^2\right\} - K_z\frac{g}{\theta}\left[\frac{\partial \theta}{\partial Z} - \gamma\right]$$

$$-\frac{\phi C_E E^{3/2}}{i} + \sigma_E \frac{\partial}{\partial Z}\left[K_z \frac{\partial E}{\partial Z}\right]$$

The quantity γ accounts for the counter gradient heat fluxes that would be present in a convective phase (Luc Musson-Gennon, 1987).

$$\gamma = C_g \frac{Q_o}{\left[-\frac{g}{\theta_*}U_*\theta_* h\right]^{1/3} \cdot h}$$

U_* and θ_* are computed using the equations described by Estoque (1963).

COMPUTATION OF THE SURFACE TEMPERATURE

For computing the surface temperature, the equation based on the force restore method is used (Deardorff, 1978). The equation for the force restore method is

$$\frac{\partial \theta_o}{\partial t} = -2\pi^{\frac{1}{2}} H_A / \left[\rho_s C_s d\right] - 2\pi\left[\theta_o - \theta_g\right]/\tau$$

The net energy flux H_A is

$$H_A = F_1 + F_2 + F_3 - F_4 - F_5$$

where F_1 is the upward long wave flux, F_2 is the sensible heat flux, F_3 is the latent heat flux, F_4 is the short wave flux and F_5 is the downward long wave radiation flux. These are computed in the following manner:

$$F_1 = E_g \sigma \theta_o^4$$

$$F_2 = \rho_a C_P C_{H_O} U_a (\theta_o - \theta_a)$$

$$F_3 = L\rho_a C_{H_O} U_a \alpha \left[q_{sal}[\theta_o] - q_a\right]$$

$$F_4 = (1 - \alpha_g) I_\infty (\sin\phi \sin\delta + \cos\phi \cos\delta \cos\psi)$$

$$F_5 = \left[\sigma_o + (1 - \sigma_o) 0.67 (1670 q_a)^{0.08}\right] E_g \sigma \theta_a^4$$

The grid domain

The grid network consists of 17 points along Z. The grid spacing is uneven (Table 1), with higher resolution near the ground.

Table 1. Heights of grid points

J	Z(meters)	J	Z(meters)
1	0	11	4000
2	10	12	5000
3	100	13	6000
4	250	14	7000
5	500	15	8000
6	700	16	9000
7	1000	17	10000
8	1500		
9	2000		
10	3000		

The finite difference equations are based on forward time, upstream space difference scheme.

INITIAL AND BOUNDARY CONDITIONS

The values of the velocity, temperature, turbulent kinetic energy (TKE) temperature and dust concentration fields are prescribed initially. The values of the component U are taken as 25, 20, 15, 10 and 5 ms^{-1}, while the V component is set equal to 0.1 ms^{-1}. The particular value of U which is used corresponds to strength of the flow in a given experiment (to be described in the next section). The temperatures are taken from a sounding in Kuwait. The initial turbulent kinetic energy (TKE) is taken as zero. The Coriolis parameter corresponding to the latitude of 29°(Kuwait) is used.

The velocity field U and V are set equal to zero at the lower boundary and are constant at the upper boundary. The other variables are also prescribed as constant at this boundary. The surface temperature is predicted in the model as prescribed above. Instead of prescribing the dust concentration C at the ground, the flux from the ground is prescribed. The expression which is used is

$$F_a = 2.15 \times 10^{-6} U_*^{4.3} \mu g \text{ cm}^{-2}\text{s}^{-1}$$

This is based on Gillette's formula (1979). An alternative way of incorporating the dust flux from the ground has been suggested by Berkofsky (1986). We plan to incorporate this suggestion in future versions of model. Initially E and C are specified at zero at all levels.

The E at the bottom level of the atmosphere is

$$E = \frac{U_*^2}{0.3}$$

while at the top it is zero.

4. Design of the experiments

One of the objectives of this investigation is to determine the dependence of dust concentration on the prevailing wind speed and the dust particle size distribution. In order to achieve this objective we have designed several experiments. In these experiments we integrated the model by using different values of the prevailing wind speed or the dust particle size. In the first series of the experiments, the effect of the wind speed is studied. For this purpose, several runs are made by using different wind speeds (Table 2). In all these runs a constant value of the dust particle size is used in order to isolate the effect of the wind speed. The next series of the experiments will study the effect of the dust particle size which is incorporated through its dependence on the settling velocity (Table 3). This settling velocity is needed in the integration for computing the equation for dust concentration (Equation 4). The effect of the dust size is determined by integrating the model using different settling velocities but with constant wind speed.

Table 2. Summary of numerical experiments.

Cases	Types of Experiments	Settling Velocity ($cm\ s^{-1}$)	Wind Speed ($m\ s^{-1}$)	Soil Temp K	Thermal Stability
1	Control	-10.0	15	301	
2	Wind	-10.0	25	301	(Based on
3	Speed	-10.0	20	301	Kuwait
4		-10.0	10	301	Sounding)
5		-10.0	5	301	
6	Settling	-5.0	15	301	
7	Vel	-1.0	15	301	
8		-0.5	15	301	

For comparison purposes, a control run is made. The initial conditions for this run are corresponding to the above mentioned case study of a dust storm. Other experiments are conducted by keeping all the variables and initial/boundary conditions exactly the same as the control experiment except for the particular variable or parameter which is being investigated.

Table 3. Dust settling speed in relation to the dust particle size (after Berkofsky, 1982).

Settling Vel. ($cm.\ s^{-1}$)	Diameter of Particle (mm)	Phenomena
-20.0 to -10.0	10^{-1} (100μ)	Sand Particles
-5.0 to -1.0	$10^{-2}(10\mu)$	Dust Particles
-0.5	$10^{-3}(1\mu)$	Fine Dust

5. Results and discussions

The control experiment

As mentioned earlier, the control experiment is going to be used for comparison purposes; therefore, the initial values used in this model are approximately similar to the observational case study of a dust storm done in Kuwait (Section 1). The integrations start at 1200 LT midnight and the model is run for 54 hour of real time.

The initial values of U equal to 15 m s^{-1} and V equal to zero are prescribed over the entire domain except at the lower boundary where they are assumed to be equal to zero. The soil temperature is taken as 301 K. The settling velocity (Ω) is set equal to -10.0 cm s^{-1}, representing a dust particle size of (100μ) which is normally categorized as sand particles (Table 3).

Since the summer days in Kuwait are usually cloudless, this model assumes that the sky is clear.

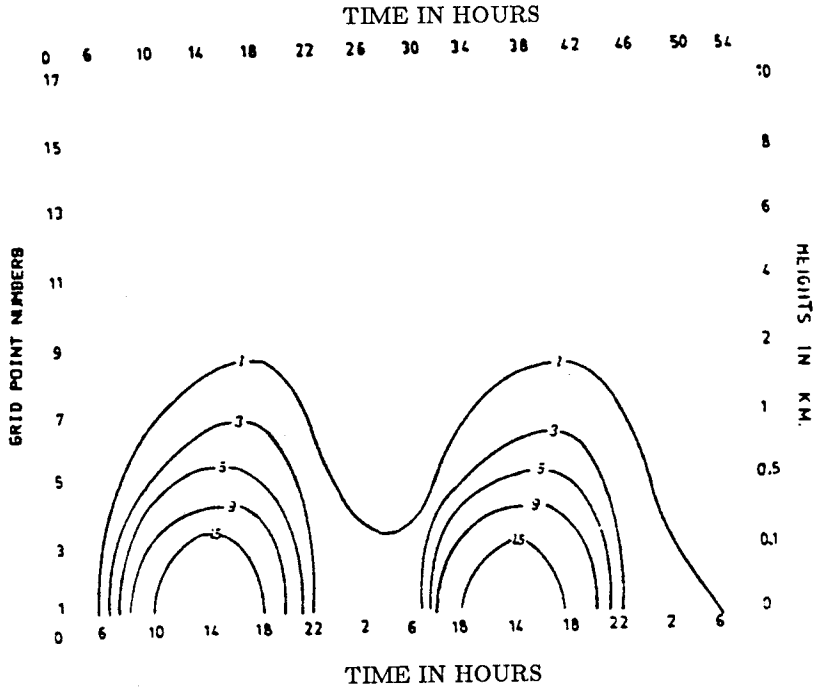

Fig. 4. Diurnal variation of dust concentration (Units, $10^3\mu$g m^{-3}) for Case No. 1 Control. Dust settling speed, 10 cm/s; prevailing wind speed, 15 m/s; soil temperature, 301 K.

Figure 4 shows the result of the control run. This figure shows a distinct diurnal pattern of dust concentration. The results show a maximum dust concentration of about $15 \times 10^3\mu$g m^{-3} during early afternoon and minimum dust concentration of about 10^3 μg m^{-3} in the early morning hours. There is also a corresponding diurnal variation of the vertical extent of dust occurrence concentration showing the maximum height of 1500 m at about 2000 LT in the evening and the minimum of 200 m by early morning. For simplicity, the vertical extent of dust occurrence is defined arbitrarily as the height which is reached by the dust concentration of 10^3 μg m^{-3}. The dust concentration rapidly increased at about 0800 LT in the morning and reached its maximum value at about 1400 LT in the afternoon. On the second day of the integrations, the same diurnal pattern of dust concentration is noticed, but is slightly less in magnitude.

The results of this control run, showing the diurnal variations of dust concentration, is in close agreement with the observed diurnal variation in Kuwait during the spell of dust storms that lasted for about nine consecutive days, from June 15 to June 24, 1973.

THE DEPENDENCE OF DUST DISTRIBUTION ON WIND SPEED

The results of the runs for different wind speeds are shown in Figs. 5 to 8; these wind speeds are 5, 10, 20, 25, ms^{-1}, respectively. The effect of the wind speed can be seen most clearly by looking at Figs. 5 and 8. In Figure 5, the prescribed wind speed is strongest at 25 ms^{-1}. In Figure 8, the wind speed prescribed is the weakest at 5 ms^{-1}. Both of these cases exhibit the diurnal variation of dust concentration. The maximum dust concentration for Figure 5 is approximately 40×10 $\mu g\ m^{-3}$ at about 1600 LT. On the other hand, the maximum dust concentration for Figure 8

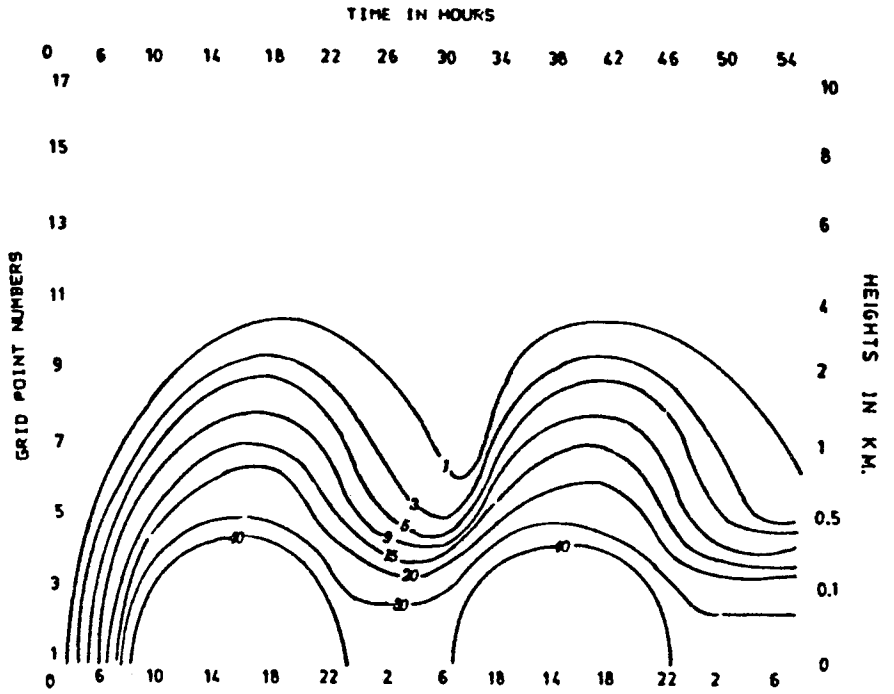

Fig. 5. Diurnal variation of dust concentration (Units, $10^3 \mu g\ m^{-3}$) for Case No. 2. Dust settling speed, 10 cm/s; prevailing wind speed, 25 m/s; soil temperature, 301 K.

is approximately 5×10^3 $\mu g\ m^{-3}$ at about 1400 LT. In Figure 5, the dust is lifted as high as 4 km during the day. During the night, the dust starts settling gradually resulting in decreased concentration of about 35×10^3 $\mu g\ m^{-3}$. By early of the next day, the dust starts rising again. In Figure 8, the dust is observed only during the day from about 0800 LT in the morning to about 1900 LT in the evening. The maximum dust concentration is about 5×10^3 $\mu g\ m^{-3}$ at about 1400 LT; and the dust is lifted to the height of about 250 meters. There is practically no dust at night time; however note in Figure 5 that dust persists at night. In Figure 6, where the wind speed is 20 ms^{-1}, almost the same diurnal pattern is observed as that in Figure 5,

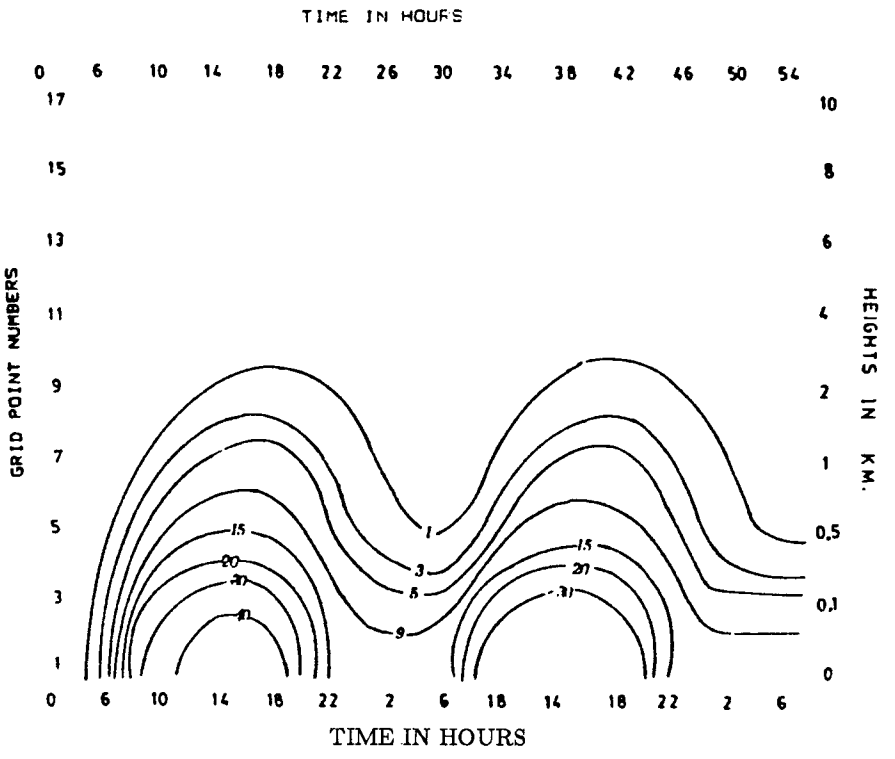

Fig. 6. Diurnal variation of dust concentration (Units, $10^3 \mu g\ m^{-3}$) for Case No. 3. Dust settling speed, 10 cm/s; Prevailing wind speed, 20 m/s; soil temperature, 301 K.

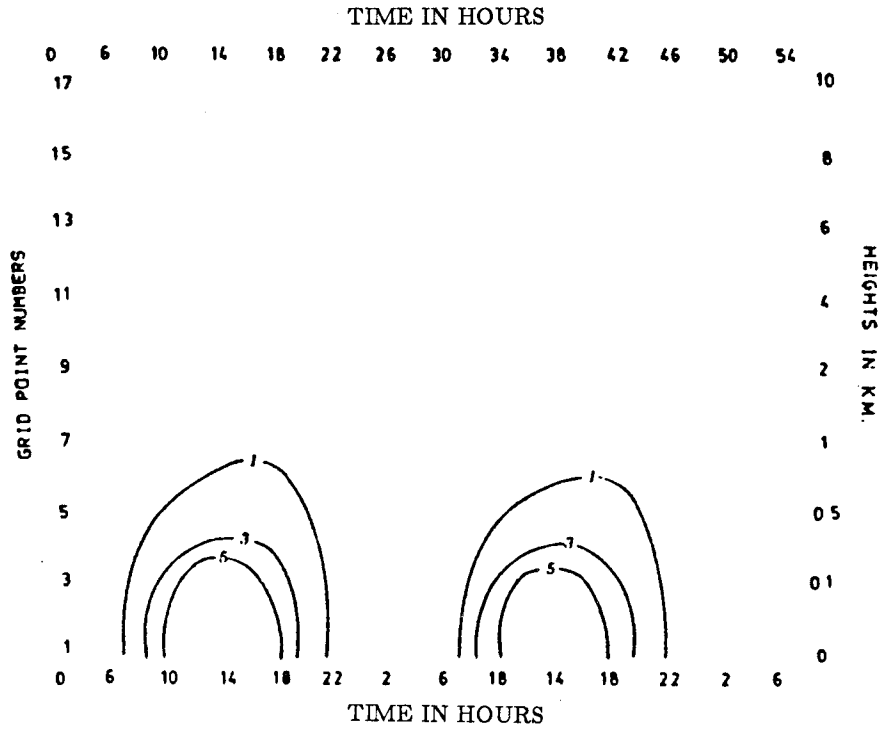

Fig. 7. Diurnal variation of dust concentration (Units, $10^3 \mu g\ m^{-3}$) for Case No. 4. Dust settling speed, 10 cm/s; prevailing wind speed, 10 m/s; soil temperature 301 K.

but with smaller values of dust concentration and the maximum height of dust concentration is about 3 km. In Figure 7, where the prevailing wind is 10 ms^{-1}, a significant decrease in dust concentration is noticed. The maximum of concentration of dust is about 5×10^3 μg m^3 about 1400 LT. At this time, the dust effectively reaches the height of about 800 meters. In Figure 7, it can be seen that the high dust concentrations existed only during the day and decreasing in intensity to practically no dust during the night. Thus, from this experiment, it can be seen that the effect of the prevailing wind speed on dust concentration is highly significant. When the prevailing wind speed is stronger, most dust is lifted from the ground and raised to the higher layers of the atmosphere by the turbulent kinetic energy. Furthermore, dust continues to exist at night time. As the prevailing winds weaken, less dust seem to be lifted to the ground; there is no dust at night.

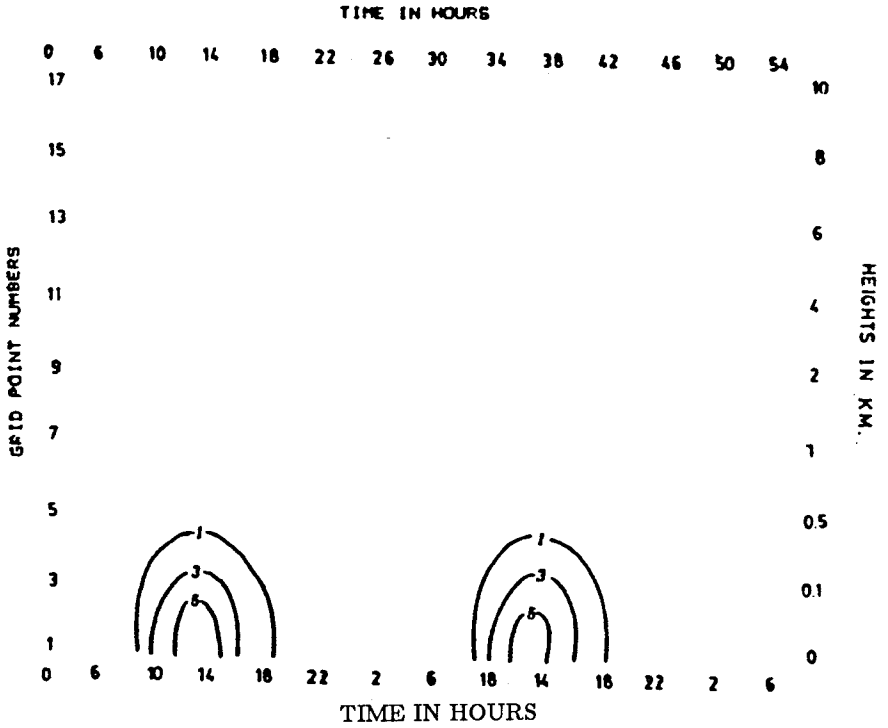

Fig. 8. Diurnal variation of dust concentration (Units, $10^3 \mu g\ m^{-3}$) for Case No. 5. Dust settling speed, 10 cm/s; prevailing wind speed, 5 m/s; soil temperature, 301 K.

THE DEPENDENCE OF DUST DISTRIBUTION ON DUST PARTICLE SIZE

In this experiment, the effect of the dust particle size through its relationship with the settling velocity is studied (Table 3). Figs. 9 to 11 show the dependence of the distribution of dust on dust particle size. These figures exhibit again the diurnal variation of dust concentration. The effect of dust size can be seen most clearly by comparing Figure 11, where the settling velocity prescribed is -0.5 cm s^{-1}, with that of the control experiment (Fig. 4), where the settling velocity used was -10 cm s^{-1}. It can be noticed that the control experiment shows a more distinct diurnal variation of dust concentration. Figure 11 shows only a slight diurnal variation as the dust is present throughout day and night. Figure 11 also shows that the maximum dust concentration occurred about 1600 LT and is approximately 40×10^3 μg m^{-3}. The dust concentration reached

the maximum height of about 5.5 km. In the control experiment, the maximum height reached is about 1.8 km. It is also noticed that the dust went higher on the second day than on the first day of the integrations. This could be explained by the fact that much of the dust lifted during the previous day has not yet settled down and is accumulated on the next day. In Figure 9, the settling velocity prescribed is -5 cm s^{-1}, which represent the dust particle size of 10 μ. Here, it can be noticed that the dust concentration increased in intensity and the dust particles reached the height of about 3 km, whereas in the control experiment, the dust particles reached the height of about 1800 meters. The maximum dust concentration of approximately 20×10 μg m^{-3} occurred at about 1400 LT. After 2000 LT in the evening the dust concentration gradually starts to decrease till 0800 LT in the morning of the next day. Subsequently, it increases during the day, following the same diurnal pattern of the previous day and showing suspended dust at night. In Figure 10, where the settling velocity used is -1.0 cm s^{-1} representing the dust particle size of 1 μ, dust variation is almost similar to that of Figure 11.

The experiment shows that dust particle size has a significant effect in the dust phenomena. The smaller the dust particles are, the higher they tend to rise; moreover, the dust tends to remain suspended in the atmosphere and to accumulate in the successive days. It can also be seen that, the finer the dust particle, the smaller is the diurnal variation of dust concentration.

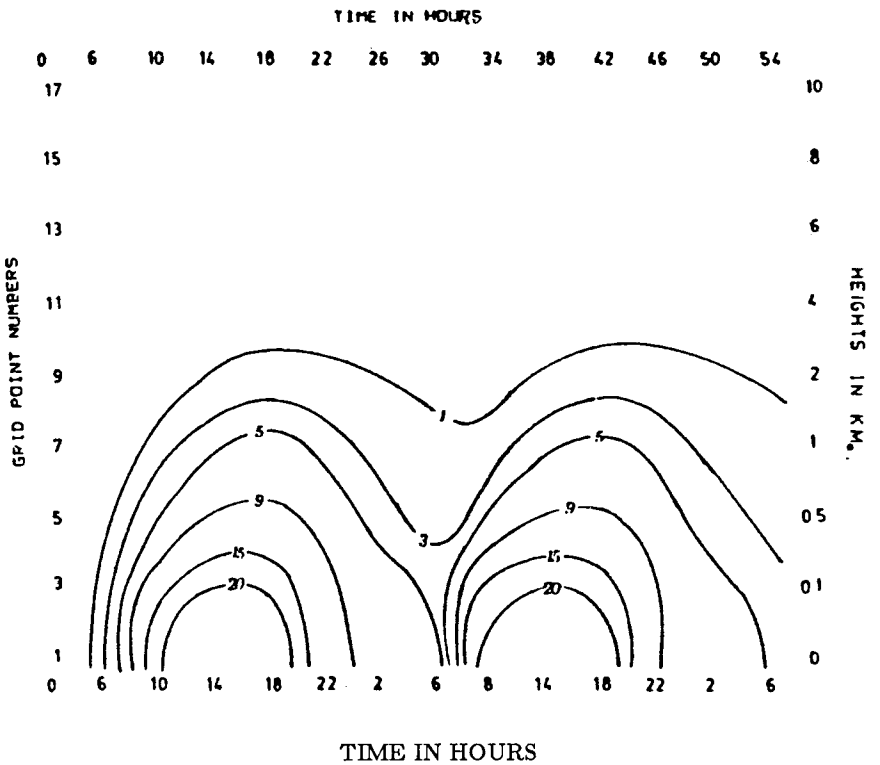

Fig. 9. Diurnal variation of dust concentration (Units, $10^3 \mu g\ m^{-3}$) for Case 6. Dust settling speed, 5 cm/s; prevailing wind speed, 15 m/s; soil temperature, 301 K.

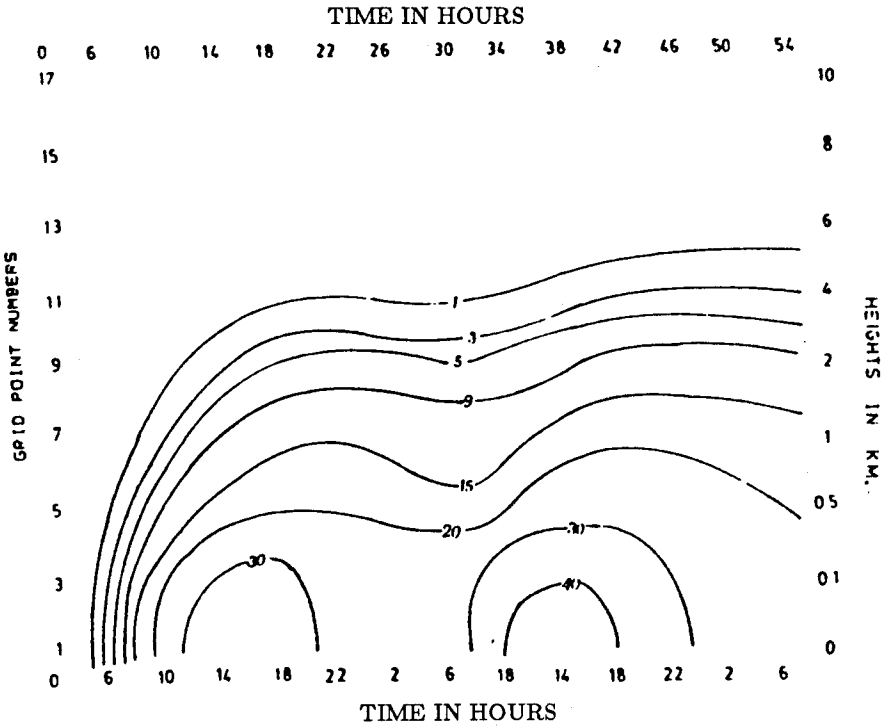

Fig. 10. Diurnal variation of dust concentration (Units, $10^3 \mu g\ m^{-3}$) for case No. 7. Dust settling speed, 1 cm/s; prevailing wind speed, 15 m/s; soil temperature, 301 K.

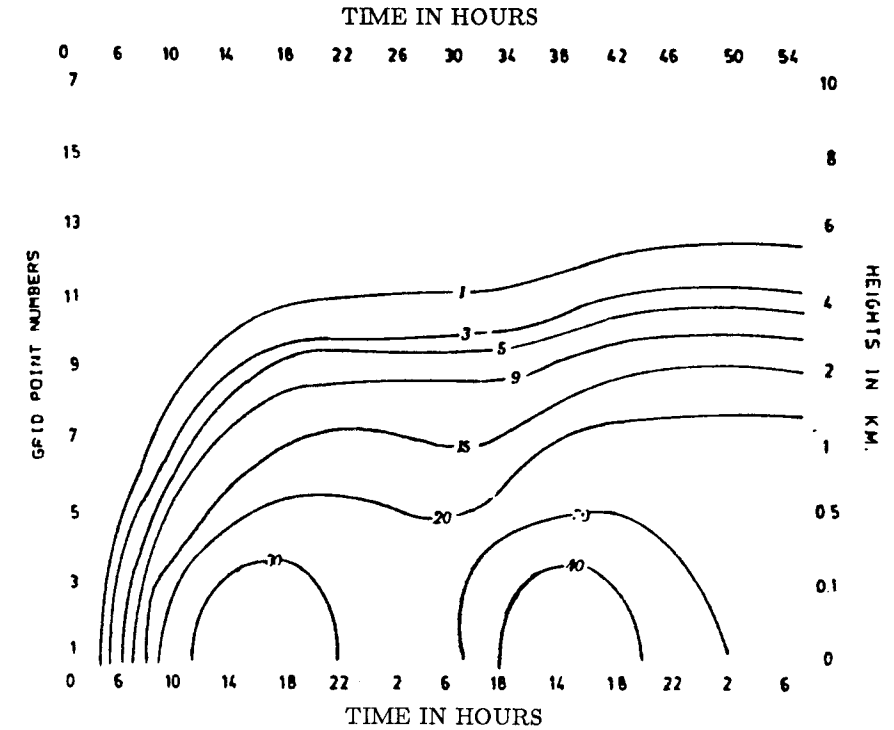

Fig. 11. Diurnal variation of dust concentration (Units, $10^3 \mu g\ m^{-3}$) for Case No. 8. Dust settling speed, 0.5 cm/s; prevailing wind speed, 15 m/s; soil temperature, 301 K.

6. Summary and conclusions

In this paper, we have described a dust model over homogeneous terrain. The model has been integrated in order to simulate dust observations over Kuwait. The simulations appear to be realistic, reproducing the observed diurnal observations with maximum occurrence of dust during the daytime. We have used the model to study the effects of wind speed and dust particle size on dust concentrations. The results of this study may be summarized as follows:

a) The wind speed is one of the most important factor for the generation of dust. When the prevailing winds are stronger, more dust is lifted from the ground and raised to the higher layers of the atmosphere. As the prevailing winds weaken, less dust tend to be lifted from the ground.

b) With respect to the effect of dust particle size, the smaller the dust particles are, the higher the concentration is and the higher they tend to rise. Furthermore they tend to remain suspended in the atmosphere for many successive days.

APPENDIX
LIST OF SYMBOLS AND CONSTANTS

a_o	empirical constant = 0.2
C	dust content of the air
C_E	empirical constant = 0.08
C_g	countergradient constant of the atmosphere which is equal to 2×10^{-12}
C_{HO}	heat transfer coefficient = 0.0025
C_S	specific heat of the soil = 0.24 cal g^{-1} $°K^{-1}$
C_P	specific heat of air at constant pressure = 0.24 (cal g^{-1} $°K^{-1}$)
E	turbulent kinetic energy (TKE)
E_g	emissivity of the ground = 0.82
F_1	upward long wave flux
F_2	sensible heat flux
F_3	latent heat flux
F_4	shortwave flux
F_5	downward long wave radiation flux
f	Coriolis parameter = 0.7×10^{-4} (for Kuwait)
g	acceleration due to gravity = 980.6 cm s^{-2}
H	height of the domain
H_A	total incoming and outgoing energy fluxes
I_∞	solar constant = 1.95 cal cm^{-2} min^{-1}
i	in grid domain stands for horizontal index
j	in grid domain stands for vertical index
k	von Karman constant = 0.41
K_s	soil heat diffusivity constant = 3×10^{-3} $cm^2 s^{-1}$
K_z	vertical diffusion coefficient
L	latent heat of vaporization = 540 cal g^{-1}
l	mixing length
l_∞	asymptotic mixing length = 25 meters
P_o	= 1000 hPa
P	pressure
Q_o	soil kinematic heat flux
q_{sat}, q_a	mixing ratio at computed ground temperature and at computed air temperature respectively = 0.032 g/g
R	gas constant for dry air
Ri	Richardson number
T	absolute temperature
T_a	air temperature
T_*	characteristic temperature

T_g	ground temperature
t	time
U	component of the wind in x direction
U_a	wind velocity at anemometer level
U_*	friction velocity
U_g	x component of the geostrophic wind
V	component of the wind in y direction
W_*	convective scale
Z_o	roughness parameter = 0.0031 cm
α	soil moisture parameter = 0.6
α_g	ground albedo (For dry sandy desert = 0.35)
α_s	stability parameter for stable case = 7.0
α_N	stability parameter for unstable case = 0.5
δ	solar declination
γ	lapse rate
σ	Stephan-Boltzman constant = 8.128×10^{-11}
σ_o	cloud fraction
σ_E	empirical constant = 1.2
θ	potential temperature
θ_o	surface temperature
θ_g	temperature at the bottom of the soil (10 cm)
$\Omega(r)$	sedimentation or settling velocity of dust particles of radius r
ϕ	latitude (Kuwait $\phi = 29°$N)
Φ	stability function
ψ	hour angle
ρ, ρ_a	density of the air
ρ_s	soil density = 2.65 g cm^{-3}
τ	diurnal period = 1440 min.

Acknowledgement

The authors wish to thank the meteorological departments of Democratic Yemen and State of Kuwait for providing the necessary data required for this study

REFERENCES

Al-Kulaib, A., 1984. The Climate of Kuwait. Climatological Dept., Meteorological Dept., Directorate of Civil Aviation, Kuwait, 178 pp.

Berkofsky, L., 1982. A Heuristic Investigation to evaluate the feasibility of developing a desert dust prediction model. *Mon. Wea. Rev.*, **110**, 2055-2062.

Berkofsky, L., 1986. The problem of wind erosion arising in a mesoscale prediction model. Proc. WMO/IUGG NWP Symposium, Tokyo, 199-209.

Deardorff, J. W., 1966. The counter-gradient heat flux in the lower atmosphere and in the laboratory. *J. Atmos. Sci.*, **23**, 503-506.

Deardorff, J. W., 1970. Convective velocity and temperature scales for the unstable planetary boundary layer and for Rayleigh convection. *J. Atmos. Sci.*, **27**, 1211-1213.

Deardorff, J. W., 1970. Preliminary results from numerical integrations of the unstable planetary boundary layer. *J. Atmos. Sci.*, **27**, 1209-1211.

Deardorff, J. W., 1982. Efficient prediction of ground surface temperature and moisture, with inclusion of layer of vegetation. *J. Geof. Res.*, Vol. **83**, No. 64, 1989-1993.

El-Fandy, M. G., 1953. On the physics of the dust atmosphere. *Q. Jour. Roy. Meteor. Soc.*, **79**, 284-287.

El-Mashjary, M. S., 1990. Numerical simulation of dust occurrence in the atmosphere. Ph. D. Thesis, Department of Meteorology and Oceanography, College of Science. University of the Philippines, Diliman, Quezon City.

Estoque, M. A., 1963. A numerical model of the atmosphere boundary layer. *J. Geophys. Res.*, Vol. **68**, No. 4, 1003-1013.

Estoque, M. A. and C. M. Brumralkar, 1969. Flow over a localized heat source. *Mon. Wea. Rev.*, **97**, 850-859.

Estoque, M. A., J. Gross and H. W. Lai, 1976. A lake breeze over Southern Lake Ontario. *J. Atmos. Sci.*, **19**, 244-250.

Gillete, D. A., 1979. Environmental factors affecting dust emission by wind erosion. In Saharan Dust, Scope Report 14, C. Morales, Ed., John Wiley and Sons, N. Y., 119-131.

Gross, G., 1987. Some effects of deforestation on nocturnal drainage flow and local climate - A numerical Study, *Boundary-Layer Meteorology*, **38**, 315-337.

Mellor, G. L. and T. Yamada. A hierarchy of turbulence closure models for planetary boundary layers. *J. Atmos. Sci.* Vol. **31**, 1791-1806.

Musson-Gennon, Luc, 1986. Numerical simulation of a fog event with a one-dimensional boundary layer model. *Mon. Wea. Rev.*, **115**, 592-607.

Safar, M. I., 1985. Dust and dust storms in Kuwait; Meteorological Dept. Directorate of Civil Aviation, Kuwait, 189 pp.